$$\text{Parallel: } \frac{d}{dt}(Q\bar{\gamma}) = \frac{\bar{k}_p(C_A)_b(1-\bar{\gamma})}{\left[1+\sum_{i\neq A}(K_iC_i)^{m_i}\right]^n_{\text{bulk}}} \tag{22}$$

$$\text{Series: } \frac{d}{dt}(Q\bar{\gamma}) = \frac{\bar{k}_p(C_B)_b(1-\bar{\gamma})}{\left[1+\sum_{i\neq B}(K_iC_i)^{m_i}\right]^n_{\text{bulk}}} \tag{23}$$

Reaction stoichiometry allows an expression of $(C_B)_b$ in terms of $(C_A)_b$ for use in the equations developed. The equations necessary for the transformation of the heterogeneous reactor problem to a homogeneous one are also summarized in Table 1.

CONCLUDING REMARKS

Global rates have been developed for the reactions limited by diffusion and affected by deactivation intermediate between uniform and shell-progressive. These global rates allow the treatment of a heterogeneous reactor design problem with deactivation as a homogeneous one. The global rates obtained, however, are not applicable to the entire space of the intermediate deactivation regime but rather limited to a subspace in which the pellet center concentration approaches zero (diffusion-limited reactions) and the pellet surface activity does not approach zero such that the condition of Eq. 2 (or Eq. 2a for an nth-order reaction) is satisfied. For diffusion-limited reactions being considered, the condition of Eq. 2 is usually met as Eq. 2a indicates unless the surface activity is quite small. In such cases, more terms can be added to the flux expression of Eq. 1 (Lee, 1981a).

NOTATION

C = concentration of key species
C_b = bulk concentration
C_c = pellet center concentration
C_A = concentration of species A
C_B = concentration of species B
D_e = effective diffusivity of key reactant
D_p = effective diffusivity of poisoning species
f = activity distribution function
f' = df/dx
g = concentration dependence of the rate of main reaction
$G(c)$ = product inhibition term in kinetics of poisoning reaction
h = film heat transfer coefficient
$H(C_b)$ = function defined by Eq. 16
$(-\Delta H)$ = heat of reaction
J = function defined by Eq. 14
k = rate constant of main reaction
k_b = k evaluated at T_b
k_p = rate constant of poisoning reaction
k_s = k evaluated at T_s
L = characteristic dimension of pellet
n = order of reaction; constant in Eq. 15
N = concentration of poisoning species
P = dC/dx
Q = poisoning capacity of pellet in moles poisoning species per pellet volume
r_c = intrinsic kinetics of main reaction (= $kg(C)$)
r_p = intrinsic kinetics of poisoning reaction
$\mathcal{R}$ = global rate of main reaction based on pellet volume
$\mathcal{R}_p$ = global rate of poisoning reaction based on pellet volume
T = temperature
x = pellet coordinate
y = $1-\bar{\gamma}$

Greek Letters

γ = fraction of catalyst deactivated
ϵ = Arrhenius number, E/RT_b
ϵ_p = E_p/RT_b
$\mathcal{E}$ = reactor point effectiveness defined by Eq. 11
η_i = internal effectiveness factor defined by Eq. 6
$(\eta_i)_p$ = internal effectiveness for poisoning reaction given by Eq. 17
ϕ = Thiele modulus, $L(kC_b^{n-1}/D_e)^{1/2}$

Subscripts

b = bulk fluid
c = pellet center
s = pellet surface

LITERATURE CITED

Lee, H. H., "Generalized Effectiveness Factor for Pellets with Nonuniform Activity Distribution: Asymptotic Region of Strong Diffusion Effect," *Chem. Eng. Sci.*, **36**, 1921 (1981a).

Lee, H. H., "An Approximate Approach to Design and Analysis of Heterogeneous Catalytic Reactors," *AIChE J.*, **27**, 558 (1981b).

Lee, H. H., and J. B. Butt, "Heterogeneous Catalytic Reactors Undergoing Chemical Deactivation: II Design and Analysis: The Approach of Reactor Point Effectiveness," *AIChE J.* **28**, 410 (1982).

Lee, H. H., and J. B. Butt, "Heterogeneous Catalytic Reactors Undergoing Chemical Deactivation: I. Deactivation Kinetics and Pellet Effectiveness," *AIChE J.* **28**, 405 (1982).

Manuscript received September 22, 1981; revision received February 11, and accepted March 4, 1982.

Fine Structure of the CSTR Parameter Space

V. K. KWONG and T. T. TSOTSIS

Dept. of Chemical Engineering
University of Southern California
Los Angeles, CA 90007

In a recent communication by the same title, Williams and Calo (1981) have examined the "fine structure" of the CSTR parameter space. The authors have suggested the existence of five additional regions of stability behavior resulting by subdivision of the regions already presented by Uppal, Ray and Poore (1974) in their classical paper on "The Dynamic Behavior of a CSTR." Williams and Calo (1981) discovered the additional regions of stability behavior by considering the demarcations created in the parameter space by the coincidence of the Damkohler numbers corresponding to the roots of the trace, s_1,s_2 and of the determinant of the stability matrix

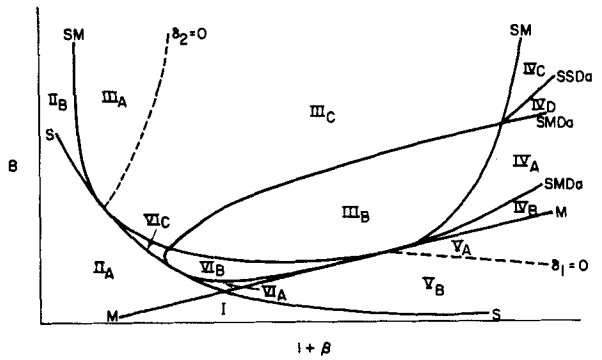

Figure 1. Classification of dynamic behavior in parameter space. A schematic plot.

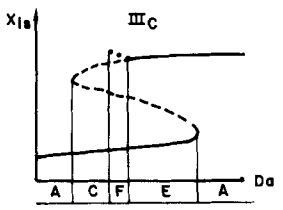

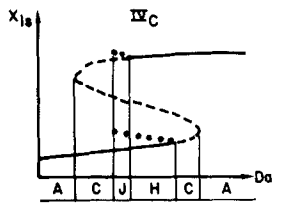

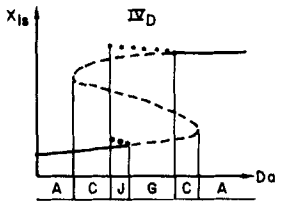

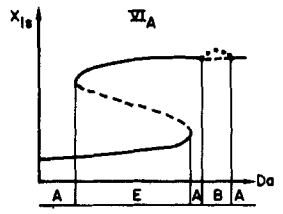

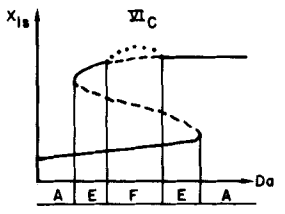

Figure 2. New conversion vs. *Da* plots as described by Williams and Calo (1981).

m_1,m_2. [For brevity, we will assume the same notation with that of Uppal et al. (1974) and Williams and Calo (1981).] Two new curves appear in the $(B, 1+\beta)$ parameter space. Along the first of these curves, which Williams and Calo call SMD_a, $Da(s_1,s_2) = Da(m_1,m_2)$, while along the second curve, curve SSD_a, $Da(s_1) = Da(s_2)$.

In Figure 1 (which is Figure 1 of Williams and Calo and is not drawn to scale to show all the regions clearly), the regions first discovered by Uppal, Ray and Poore as well as the additional new regions uncovered by Williams and Calo are shown. There are in total 15 regions of stability behavior. Ten of them were originally discovered by Uppal, Ray and Poore while the remaining five were recently discovered by Williams and Calo.

The stability behavior of the latter, i.e., regions $\mathrm{III_C}$, $\mathrm{IC_C}$, $\mathrm{IV_D}$, $\mathrm{VI_A}$, $\mathrm{VI_C}$, as described by Williams and Calo, is shown in Figure 2 (Figure 2 of Williams and Calo, 1981). The stability behavior of regions $\mathrm{III_C}$, $\mathrm{VI_A}$, $\mathrm{VI_C}$ as described by Williams and Calo (1981) is correct. However, the same is not true for region $\mathrm{IV_C}$ and $\mathrm{IV_D}$. One does not need to resort to extensive numerical investigations

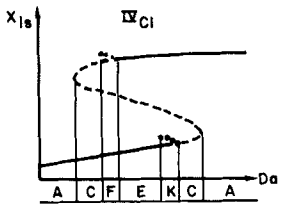

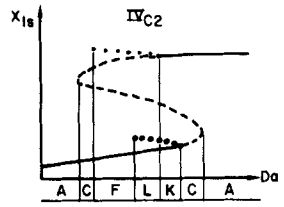

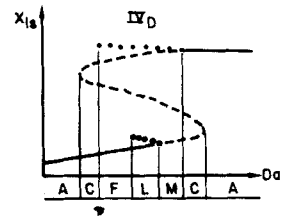

Figure 3. Correct new conversion vs. *Da* plots.

(numerical examples are presented, however, at the end of this paper to verify that in region $\mathrm{IV_C}$ a phase plot behavior of type J cannot exist, Figure 2. For a type-J behavior to exist a limit cycle must surround all three steady states, the lower state also being surrounded by a limit cycle (Uppal et al., 1974).

For reasons of solution boundness, the limit cycle surrounding all the states must be stable. Observe now the behavior of region $\mathrm{IV_C}$ as described by Williams and Calo in Figure 2. At the point where the upper limit cycle appears (the limit cycle which, for a type-J behavior, must surround all other states), i.e., $Da = Da(s_2)$, already all three steady states exist separated by the separatrices. The upper limit cycle bifurcates through a soft bifurcation point and its size at the bifurcation point is close to zero. It is impossible, therefore, for this limit cycle to surround all three steady states. The same arguments also apply to region $\mathrm{IV_D}$ of Figure 2. It can be verified rather easily that a left to right transition between a C- and a G-type behavior is impossible.

The correct dynamic behavior for regions $\mathrm{IV_C}$ and $\mathrm{IV_D}$ is shown in Figure 3. For region $\mathrm{IV_C}$ there are two types of stability behavior. The first type, which we define as $\mathrm{IV_{C1}}$, contains a new type of a phase plot which, to be consistent with previous publications on the subject, we call phase-plot type K. This phase plot is schematically shown in Figure 4. In this phase plot, there are three steady states. The upper state is stable. The low state is also stable, but it is surrounded by an unstable limit cycle. Thus, qualitatively, phase-plot type K is similar to the phase-plot type H of Uppal et al. (1974). However, in region H of Uppal et al. (1974) the upper state is the one which is surrounded by a limit cycle. It is interesting to note that in region $\mathrm{IV_{C1}}$, a type-E region (without limit cycles) is surrounded by two regions, i.e., F and K, each having a single limit cycle.

The second type of stability behavior, $\mathrm{IV_{C2}}$, also contains a new type of phase plot which we call phase-plot type L (Figure 4). Note that in this new phase plot, there are three steady states. The upper state is unstable and is surrounded by a stable limit cycle, while the low state is stable and is surrounded by an unstable limit cycle. Furthermore, the two limit cycles do not vanish at the same point.

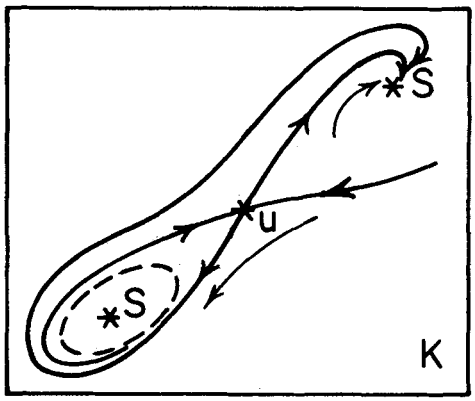

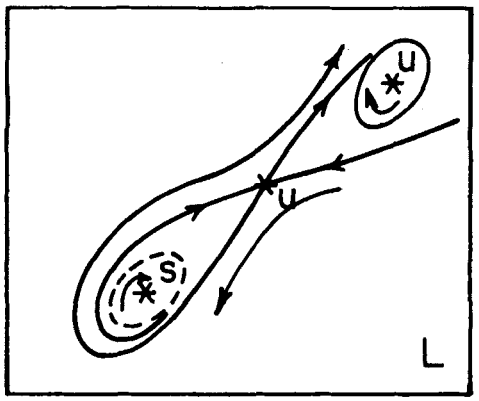

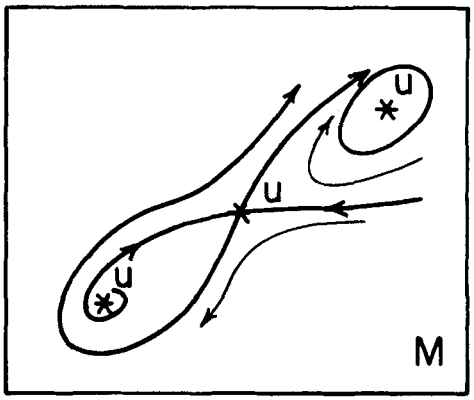

Figure 4. K- and L-type phase plots.

TABLE 1. NUMERICAL VALUES OF PARAMETERS USED IN THE EXAMPLES

Case No.	(β,B)	Region	Sign of δ_1,δ_2	(m_1,Da_{m1})	(m_2,Da_{m2})
1	(7.0,77.5)	IV_{C1}	$\delta_1 < 0, \delta_2 < 0$	0.13563,0.04570563)	(0.74309,0.01453327)
2	(7.0,76.7126)	IV_{C2}	$\delta_1 < 0, \delta_2 < 0$	(0.13733,0.04627458)	(0.74160,0.01512086)
3	(15.98,205.0)	IV_D	$\delta_1 < 0, \delta_2 < 0$	(0.10454,0.03561590)	(0.76909,0.00586904)

Case No.	(S_1,Da_{s1})	(S_2,Da_{s2})	Da^*_{s1}	Da^*_{s2}
1	(0.13395,0.04572615)	(0.96255,0.04446067)	0.045725	0.042
2	(0.13536,0.04627056)	(0.96236,0.04627035)	0.046267	0.042
3	(0.09912,0.03557331)	(0.98398,0.03560785)	0.03555	0.032

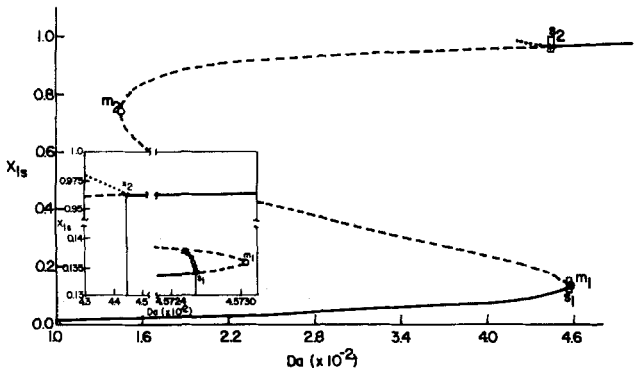

Figure 5. Steady states and limit cycles for parameters in region IV_{C1}, γ = 20 B = 77.5, β = 7.0.

The correct stability behavior of region IV_D is again shown in Figure 3. A new phase plot appears again which we define as phase-plot type M. In this phase plot (Figure 4), there are three steady states all unstable and only the upper state is surrounded by a stable limit cycle. [Note that phase plot-type C of Figure 3 does not correspond exactly to phase-plot type C of Uppal et al. (1974). In region C of Figure 3, the low state is unstable while the upper state is stable. In contrast in region C of Uppal et al. (1974), the upper state is unstable while the low state is stable. However, since both regions do not contain a limit cycle, have exactly the same number of stable and unstable states and in a sense they are mirror images of each other we do not feel that a separate notation is required.]

NUMERICAL EXAMPLES

In this chapter numerical examples will be presented verifying the existence of phase plots of type K, L and M (Figure 4) and the dynamic behavior of regions IV_{C1}, IV_{C2} and IV_D (Figure 3). The numerical values of the parameters used in the examples are shown in Table 1. These examples are part of an ongoing investigation of the dynamic behavior of lumped reactor systems obeying Arrhenius-type kinetics with finite activation energies. For the value of

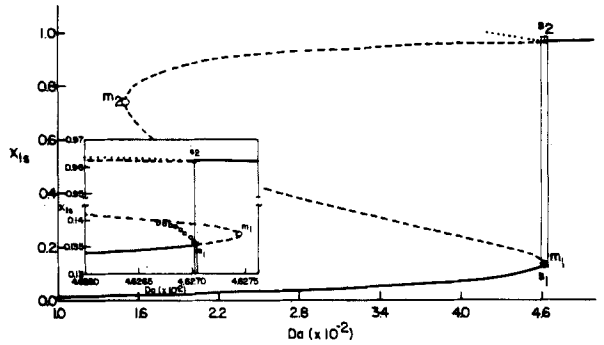

Figure 6. Steady states and limit cycles for parameters in region IV_{C2}, γ = 20 B = 76.7126, β = 7.0.

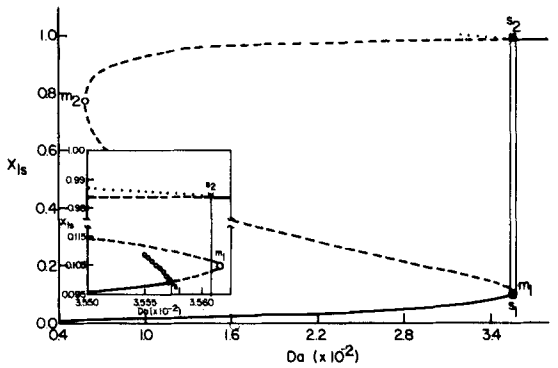

Figure 7. Steady states and limit cycles for parameters in region IV_D, γ = 20, B = 205.0 β = 15.98.

γ (γ = 20) used, however, the dynamic behavior of the CSTR is qualitatively the same with its behavior predicted for finite activation energies.

In Figure 5, the steady-state plot for IV_{C1} is shown. As it can be seen from the insert in Figure 5, there are two limit cycles. The lower limit cycle, however, disappears at a critical point Da^*_{s1} before the upper limit cycle appears [which happens for $Da = Da(s_2)$]. (See also Table 1.) In Figure 8a the phase plot for this case is shown for a value of Da in the region $(Da(s_1), Da^*_{s1})$. This is a K-type phase plot for which the stable low state is surrounded by an unstable limit cycle. In Figure 6 the steady-state plot for region IV_{C2} is shown. From the insert in this figure it can be seen that two limit cycles exist. The limit cycle surrounding the low state disappears at a critical point Da^*_{s1}. At this point, however, the upper limit cycle has already appeared ($Da^*_{s1} < Da(s_2)$) creating therefore a phase plot of type L. Figure 8b shows the L-type phase plot. Note that the two limit cycles are far apart from each other and in any event the upper limit cycle does not surround the low limit cycle. (Which would have been the case if a J-type plot, as predicted by Williams and Calo (1981), really existed.) Finally, Figure 7 shows the steady-state plot for region IV_D. The new, type-M, phase plot is shown in Figure 8c. There are three steady states, all of them unstable and the upper state is surrounded by a stable limit cycle.

CONCLUSIONS

The dynamic behavior of a CSTR-obeying Arrhenius-type kinetics with large activation energies has been reexamined. Three new types of dynamic behavior and two new phase plots have been discovered. The new additions further enrich the already intriguing dynamic behavior exhibited by this simple system.

Our ongoing investigation of this system for moderate and low activation energies has recently uncovered a few new additional

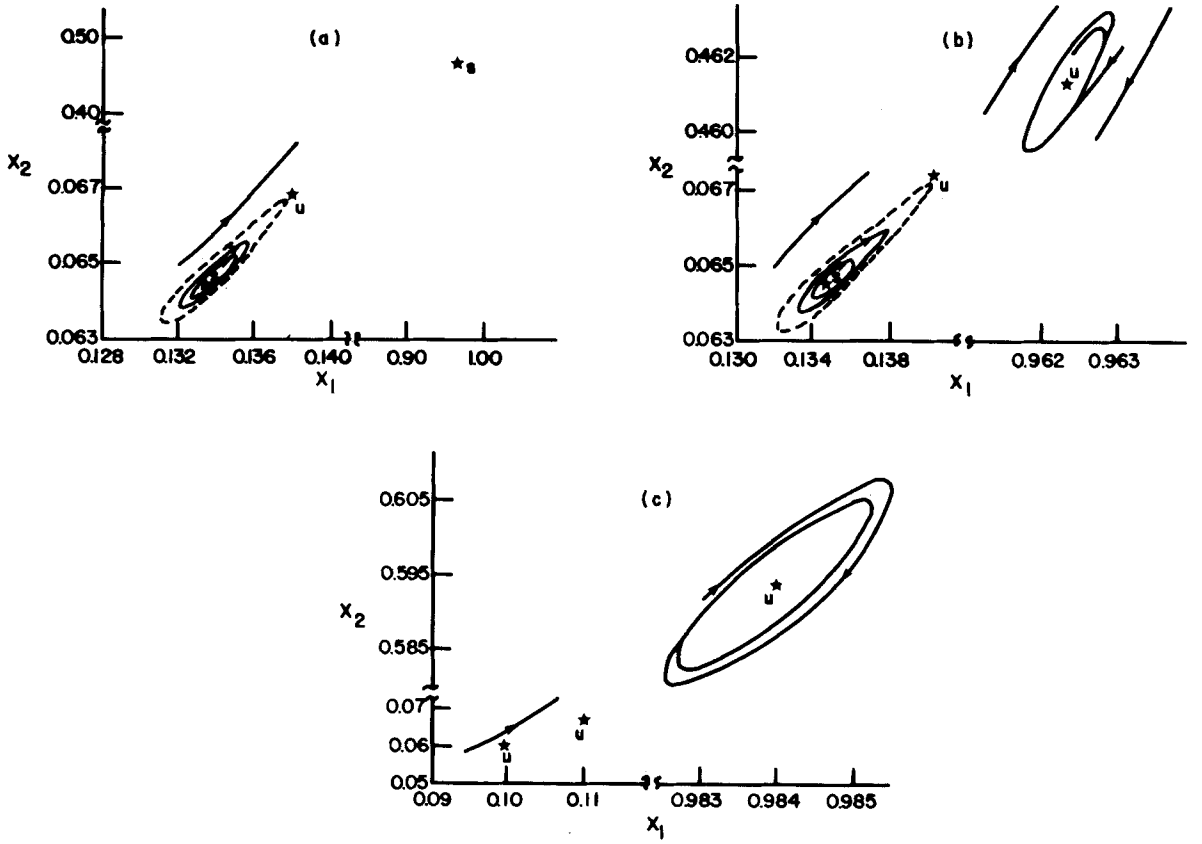

Figure 8. Phase plane trajectories: 8a. region IV_{C1}, γ = 20, Da = 0.045725 B = 77.5 β = 7; 8b. region IV_{C2}, γ = 20, Da = 0.046267, B = 76.7126, β = 7; 8c. region IV_D, γ = 20, Da = 0.03558, B = 205.0, β = 15.98.

types of stability behavior further underscoring the richness of the dynamic behavior of this system.

NOTATION

B = dimensionless adiabatic temperature rise
m_1, m_2 = roots of the determinant of the stability matrix
s_1, s_2 = roots of the trace of the stability matrix
X_{1s} = dimensionless steady-state conversion
X_{2s} = dimensionless steady-state temperature
Da = Damkohler number
β = dimensionless heat transfer coefficient
γ = dimensionless activation energy
δ_1, δ_2 = parameters defined by Uppal et al. (1974)

ACKNOWLEDGMENT

This work is a part of a project supported by the National Science Foundation (CPE-8106571).

LITERATURE CITED

Uppal, A., W. H. Ray, and A. B. Poore, "On the Dynamic Behavior of the Continuous Stirred Tank Reactor," *Chem. Eng. Sci*, **29**, 967 (1974).
Williams, D. C., and J. M. Calo, "Fine Structure of the CSTR Parameter Space," *AIChE J.*, **27**(3), 514 (1981).

Manuscript received August 10, 1981; revision received February 5, and accepted March 4, 1982.

Diaphragm Diffusion Cell: Simpler Cell Design and New Equation to Calculate Diffusivities

ABDUL-FATTAH A. ASFOUR and F. A. L. DULLIEN

Chemical Engineering Department
University of Waterloo
Waterloo, Ontario, Canada N2L 3G1

Since Northrop and Anson (1929), made the first diaphragm diffusion cell, the method proposed by them for measuring liquid diffusivities has become well established. The diaphragm cell design has undergone several modifications over the years, mainly with the purpose of eliminating various sources of error (e.g., Stokes, 1950; Dullien and Shemilt, 1961; Albright and Mills, 1965).

The first point of this note is the diaphragm cell design, Figure 1, due to Asfour (1979), which is far simpler than the most sophisticated design known to the authors, Albright and Mills (1965), but notwithstanding its simplicity, yields results of comparable precision. Both the top and the bottom plugs of the cell are made of teflon; there is a capillary bore in the top plug which permits volume changes of the liquid in the upper compartment, while the stainless-steel (SS) screw cap prevents evaporation losses. There is no bore in the bottom plug. The brass bottom cap, threaded on the inside, screws onto the brass ring glued on the extension of the lower compartment, and it assures a water-tight seal. The bottom cap fits into a mount at the bottom of the constant temperature bath containing oil, thus allowing the cells to be placed in the bath reproducibly and in a fixed position. As shown in Figure 1, each compartment contains a magnetic stirrer which in actual operation lightly touch the diaphragm. Sampling is done with the help of a hypodermic syringe fitted with a thin teflon tubing. First the upper compartment then; after inverting the cell, in the bath, the lower compartment is sampled as quickly as possible.

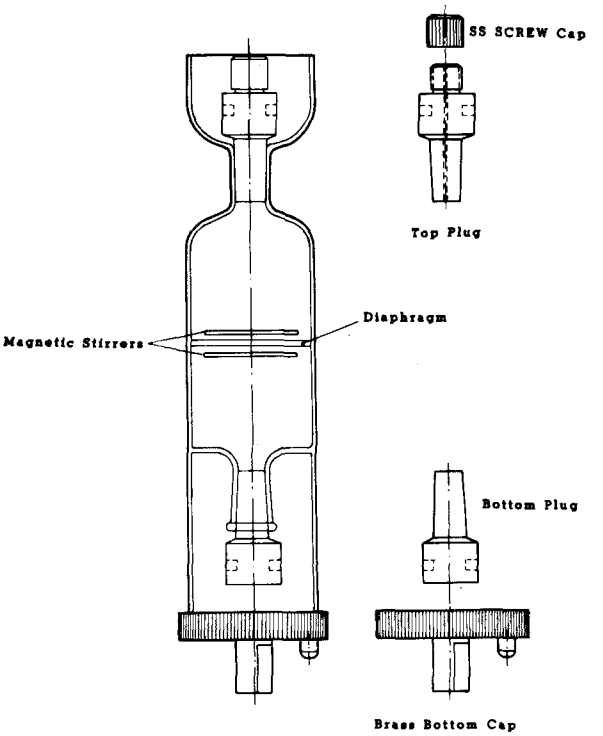

Figure 1. Diaphragm cell.

Present address of A. A. Asfour: Chemical Engineering Department, University of Windsor, Windsor, Ontario, Canada, N9B 3P4.
Correspondence concerning this paper should be addressed to F. Dullien.